Title	Short-wavelength stability analysis of thin vortex rings
Author(s)	Hattori, Yuji; Fukumoto, Y
Issue Date	2003-10
URL	http://hdl.handle.net/10228/565
Rights	Copyright © 2003 American Institute of Physics

Short-wavelength stability analysis of thin vortex rings

Y. Hattori[a)]
Department of Applied Mathematics and Theoretical Physics, University of Cambridge, Cambridge CB3 9EW, United Kingdom

Y. Fukumoto
Graduate School of Mathematics and Space Environment Research Center, Kyushu University 33, Fukuoka 812-8581, Japan

(Received 25 September 2002; accepted 16 July 2003; published 5 September 2003)

The linear stability of thin vortex rings are studied by short-wavelength stability analysis. The modified Hill–Schrödinger equation for vortex rings, which incorporates curvature effect, is derived. It is used to evaluate growth rates analytically. The growth rates are also evaluated by numerical calculation and they agree well with analytical values for small ϵ which is the ratio of core radius to ring radius. Two types of vortex rings are considered: Kelvin's vortex ring and a Gaussian vortex ring. For Kelvin's vortex ring the maximum first-order growth rate is found to be $\frac{165}{256}\epsilon$. For the Gaussian vortex ring the first-order growth rate is large in the skirts of the vortex core. The first-order instability is significant for both vortex rings. © *2003 American Institute of Physics.* [DOI: 10.1063/1.1606446]

I. INTRODUCTION

The stability of vortex rings is one of the important problems in hydrodynamic stability. Compared to the parallel flows, of which stability is studied by a number of authors, one of the characteristic features of vortex rings is that the vortex lines are curved along the ring radius. In this sense the vortex ring is one of the most fundamental objects for studying the curvature effect in hydrodynamic stability, which would manifest itself also in helical vortices, circular or, more generally, three-dimensional jets, etc.

Widnall and Tsai[1] showed by normal-mode analysis that Kelvin's vortex ring, i.e., a thin vortex ring whose vorticity in the core is proportional to the distance from the axis of symmetry, is unstable to three-dimensional disturbances (see also Widnall *et al.*[2]). This Widnall–Tsai instability is caused by the strain flow produced by the vortex ring itself. Its mechanism is essentially the same with that of the Rankine vortex in a two-dimensional strain field,[3,4] and it is recognized as the elliptical instability in the short-wave limit.[5] It is a second-order instability in the sense that the strain flow appears at the second order in ϵ which is defined as the ratio of the core radius to the ring radius. Recently we found that there exists a first-order instability for Kelvin's vortex ring and its growth rate is fairly large compared to that of the Widnall–Tsai instability.[6] One problem of using Kelvin's vortex ring is that its vorticity distribution is ideal and is not close to that of real vortex rings observed in the experiments. Unfortunately, however, it is not easy to carry out normal-mode stability analysis for realistic vortex rings.

In the short-wavelength limit, the stability analysis is reduced to solving a set of ordinary differential equations.[7,8] This local stability analysis is convenient and gives correct results for various instabilities of vortices.[5,9,10] For the cases of vortex ring with and without swirl, Lifschitz[11] showed by short-wavelength stability analysis that it seems unstable generically. He and his co-workers also calculated the growth rates for Hill's spherical vortex[11] and for a fat vortex ring with swirl[12] (see also Rozi and Fukumoto[13] for Hill's spherical vortex). For thin vortex rings, however, there are no results to the authors' knowledge.

In this paper we carry out the short-wavelength stability analysis of two types of thin vortex ring: Kelvin's vortex ring and a Gaussian vortex ring, whose leading-order vorticity is given by a Gaussian distribution. The basic flow fields of these vortex rings are given by perturbation expansion up to the second order. By virtue of perturbation expansion the first-order and second-order instabilities, which have different origins, are found separately. We calculate the corresponding growth rates both analytically and numerically. The first-order instability is shown to be significant for both vortex rings.

The paper is organized as follows. In Sec. II we derive a vortex-ring version of the Hill–Schrödinger equation which is used to evaluate the growth rate analytically. In Sec. III we show the results for Kelvin's vortex ring. Both the first-order and second-order growth rates are obtained analytically and compared to numerical results. In Sec. IV we show the results for the Gaussian vortex ring. The first-order growth rate is evaluated analytically for a general distribution of vorticity. Both the first-order and second-order growth rates are obtained numerically. Finally, we conclude in Sec. V.

II. SHORT-WAVELENGTH STABILITY ANALYSIS

We briefly summarize the method of short-wavelength stability analysis, or local stability analysis, and derive a modified Hill–Schrödinger equation for vortex rings which

[a)]Permanent address: Faculty of Engineering, Kyushu Institute of Technology, Kitakyushu 804-8550, Japan. Electronic mail: hattori@mns.kyutech.ac.jp

is used to evaluate the growth rates analytically in Secs. III and IV. Since the short-wavelength stability analysis is one of the standard methods, its details are omitted.

In the short-wavelength stability analysis, the disturbance $\boldsymbol{u}$ to the basic flow $\boldsymbol{U}$ is assumed to be in the form

$$\boldsymbol{u}=\exp\left(\mathrm{i}\frac{\Psi(\boldsymbol{x},t)}{\delta}\right)\boldsymbol{a}(\boldsymbol{x},t), \tag{1}$$

at the leading order, where δ is a small parameter. Substituting it to the linearized Euler equation for incompressible flow yields the following set of ordinary differential equations

$$\frac{\mathrm{d}\boldsymbol{X}}{\mathrm{d}t}=\boldsymbol{U}(\boldsymbol{X}), \tag{2}$$

$$\frac{\mathrm{d}\boldsymbol{k}}{\mathrm{d}t}=-\mathcal{L}^{T}\boldsymbol{k}, \tag{3}$$

$$\frac{\mathrm{d}\boldsymbol{a}}{\mathrm{d}t}=\left(\frac{2\boldsymbol{k}\boldsymbol{k}^{T}}{|\boldsymbol{k}|^{2}}-I\right)\mathcal{L}\boldsymbol{a}, \tag{4}$$

where $\mathcal{L}_{ij}=\partial U_i/\partial x_j(\boldsymbol{X})$ and the superscript T stands for transpose. The incompressibility imposes $\boldsymbol{k}\cdot\boldsymbol{a}=0$. If there exists a set of initial conditions for which $\boldsymbol{a}$ is unbounded in time, the basic flow is linearly unstable.[7,8]

We assume that the vortex ring is steady and has no swirl so that its velocity field is parallel to the cross section by a plane which includes the axis of symmetry. Then the fluid particle moves along a closed loop periodically inside the core of the vortex ring. We assume that the wavevector is periodic; the condition for periodicity is discussed later. Then the matrix in the amplitude equation (4) is periodic as well. Therefore the Floquet theory applies to the amplitude; the solution to Eq. (4) satisfies

$$\boldsymbol{a}(t+T)=\mathcal{F}(T)\boldsymbol{a}(t), \tag{5}$$

where T is a period which depends on the particle path generally and $\mathcal{F}(T)$ is the Floquet matrix. The growth rate of amplitude is determined by the eigenvalues μ_i of $\mathcal{F}(T)$ as

$$\sigma_i=\frac{\log|\mu_i|}{T}. \tag{6}$$

Thus our task is to solve either analytically or numerically Eqs. (2)–(4) and evaluate $\sigma=\max_i\sigma_i$; the basic flow is exponentially unstable if $\sigma>0$.

The amplitude equation (4) can be reduced to the Hill–Schrödinger equation as done by Bayly *et al.* for two-dimensional incompressible flows[14] and Leblanc for a two-dimensional compressible line vortex.[15] Let us take the toroidal coordinate system (r,θ,s), where s is the length along the center of the torus, and the local Cartesian coordinate system (x,y,z) centered on $r=s=0$ for a vortex ring as shown in Fig. 1. The expressions below are valid both in the toroidal coordinate system generally and in the Cartesian coordinate system for the section $z=0$. The length is nondimensionalized by the ring radius and scaled by a small but finite parameter ϵ, which is the ratio of the core radius to the ring radius. Then the amplitude equation is represented for the case of vortex rings as

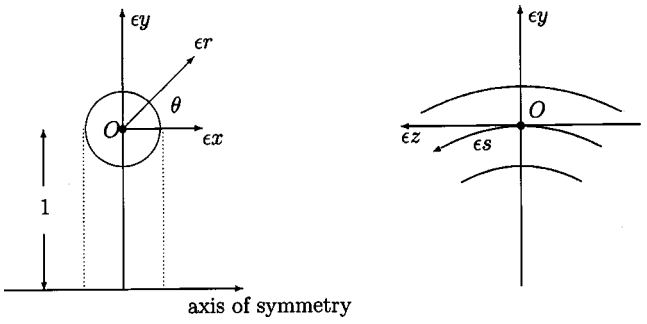

FIG. 1. Coordinate systems.

$$\frac{\mathrm{d}}{\mathrm{d}t}\begin{pmatrix}p\\q\end{pmatrix}=\begin{pmatrix}\dfrac{\mathrm{d}}{\mathrm{d}t}\log\dfrac{k_\perp}{k}+\mathrm{tr}\mathcal{L}_\perp & \dfrac{2\rho k_\parallel^2\boldsymbol{k}_\perp\mathcal{H}\boldsymbol{k}_\perp^{T}}{k_\perp^2k^2}\\ -\dfrac{\omega_s}{\rho} & -\dfrac{\mathrm{d}}{\mathrm{d}t}\log\dfrac{k_\perp}{k}-\mathrm{tr}\mathcal{L}_\perp\end{pmatrix}\begin{pmatrix}p\\q\end{pmatrix}, \tag{7}$$

where $\perp$ and $\parallel$ imply the projection to $r\theta$- or xy-plane and s or z component, respectively, ω_s is the s component of vorticity while the r and θ components are zero, $\rho=1+\epsilon y$ is the distance from the axis of symmetry of the vortex ring, and

$$k=|\boldsymbol{k}|,\quad k_\perp=|\boldsymbol{k}_\perp|,\quad k_\parallel=|\boldsymbol{k}_\parallel|,$$

$$p=\frac{k}{k_\perp}\rho\boldsymbol{k}_\perp\cdot\boldsymbol{a}_\perp,\quad q=\frac{k}{k_\perp}(\boldsymbol{k}_\perp\times\boldsymbol{a}_\perp)\cdot\boldsymbol{e}_\parallel,$$

$$\mathcal{H}=\mathcal{L}_\perp\begin{pmatrix}0 & 1\\ -1 & 0\end{pmatrix},$$

$\boldsymbol{e}_\parallel$ = unit vector in s- or z-direction.

Equation (7) is a vortex-ring version of Eq. (2.12) of Bayly *et al.*[14] Eliminating p from it, we obtain

$$\frac{\mathrm{d}^2q}{\mathrm{d}t^2}+V(t)q=0, \tag{8}$$

where

$$V(t)=\frac{2\omega_sk_\parallel^2\boldsymbol{k}_\perp^{T}\mathcal{H}\boldsymbol{k}_\perp}{k_\perp^2k^2}+\left[\frac{\mathrm{d}^2}{\mathrm{d}t^2}\left(\log\frac{k_\perp}{k}\right)+\frac{\mathrm{d}}{\mathrm{d}t}(\mathrm{tr}\mathcal{L}_\perp)\right]-\left[\frac{\mathrm{d}}{\mathrm{d}t}\left(\log\frac{k_\perp}{k}\right)+\mathrm{tr}\mathcal{L}_\perp\right]^2. \tag{9}$$

This is the Hill–Schrödinger equation for thin vortex rings. Note that there are additional terms $\mathrm{tr}\mathcal{L}_\perp$ and its derivative in Eq. (9); this is due to the curvature of the vortex ring.

Before going to particular cases, we remark on the periodicity of the wavevector. In the derivation above, we have assumed that the wavevector is periodic. For a general steady basic flow, there are two types of wavevector solution: one is periodic and the other grows algebraically. The latter is often discarded since it does not give rise to exponential instability. The periodicity is rigorously satisfied when the initial wavevector satisfies

$$\boldsymbol{U}(\boldsymbol{X}(0))\cdot\boldsymbol{k}(0)=0. \tag{10}$$

For a Gaussian vortex ring, we impose Eq. (10). For Kelvin's ring, however, the wavevector is periodic up to $O(\epsilon)$ for any initial condition. Thus we consider both the case with Eq. (10) and the case without Eq. (10).

III. STABILITY OF KELVIN'S VORTEX RING

A. Analytical results for growth rates

Here we calculate the growth rate for Kelvin's vortex ring. We use the Cartesian coordinate system here. Of course, the following calculation can be made in the coordinate system (r,θ,s), but there arises a singularity when we evaluate the second-order growth rate; in fact this singularity can be removed by choosing the stagnation point, relative to the comoving frame, as the origin, but we prefer to use the expression of the basic flow by Widnall and Tsai.[1] The velocity field and the vorticity of Kelvin's vortex ring is represented as

$$\boldsymbol{U}=\begin{pmatrix} -y \\ x \\ 0 \end{pmatrix}+\epsilon\begin{pmatrix} \frac{5}{8}-\frac{5}{8}x^2-\frac{7}{8}y^2-\frac{1}{2}z^2 \\ \frac{1}{4}xy \\ xz \end{pmatrix} + \epsilon^2\begin{pmatrix} Ay+\frac{3}{16}x^2y+\frac{1}{16}y^3-\frac{3}{8}yz^2 \\ Ax+\frac{1}{16}x^3+\frac{3}{16}xy^2-\frac{3}{8}xz^2 \\ -\frac{3}{4}xyz \end{pmatrix}, \tag{11}$$

$$\omega_s=2\rho=2(1+\epsilon y), \tag{12}$$

up to the second order in ϵ, where $A=(15/16)-(3/4)\log 8/\epsilon$ (see Appendix A). Equations (2) and (3) with the basic flow above are solved up to $O(\epsilon^2)$; see Appendix A for the details.

First, let us consider the first-order growth rate. We do not impose Eq. (10) since the wavevector is periodic up to the first order for general ϕ, which is the angle between an initial wavevector and the outward normal vector to a streamline. By substituting the solutions $\boldsymbol{X}(t)$ and $\boldsymbol{k}(t)$ to Eq. (9), the potential $V(t)$ of the Hill–Schrödinger equation (8) becomes

$$\begin{aligned} V(t)=&4(1-\sin^2\chi) \\ &+\epsilon r_0\left[\left(\frac{15}{2}-\frac{37}{2}\sin^2\chi+12\sin^4\chi\right)\sin t\right. \\ &\left.+\left(-\frac{15}{4}-\frac{9}{4}\sin^2\chi+6\sin^4\chi\right)\sin(t+2\phi)\right] \\ &+O(\epsilon^2), \end{aligned} \tag{13}$$

where χ is the angle between the vortex core axis and $\boldsymbol{k}(0)$ and r_0 is the "$O(1)$-radius" of the orbit. According to the Floquet theory, the resonance occurs if $[4(1-\sin^2\chi)]^{1/2}=n/2$; the most important resonance occurs at $\cos\chi^{(1)}=\pm 1/4$. We restrict our attention to $0\leqslant\chi\leqslant\pi/2$ since the case of $\pi/2\leqslant\chi\leqslant\pi$ exhibits the identical behavior. By using Mathieu's method for the Hill–Schrödinger equation,[16] the corresponding growth rate is found to be

$$\sigma^{(1)}=\frac{15\epsilon r_0}{256}\sqrt{61-60\cos 2\phi}+O(\epsilon^3) \tag{14}$$

(see Appendix B for the details). Thus we have

$$\sigma^{(1)}_{\max}=\frac{165}{256}\epsilon r_0+O(\epsilon^3), \tag{15}$$

at $\phi=\pi/2$. The $O(\epsilon)$ growth rate $\sigma^{(1)}$ is maximal at $r_0=1$.

Next we consider the second-order growth rate. We set $\phi=0$ or $\pi/2$ so that the wavevector is periodic up to this order. For $\phi=0$, the potential $V(t)$ turns out to be

$$\begin{aligned} V(t)=&4(1-\sin^2\chi)+\epsilon\left(\frac{15}{4}-\frac{83}{4}\sin^2\chi+18\sin^4\chi\right)r_0\sin t \\ &+\epsilon^2\left[(1-\sin^2\chi)\left\{5+\left(-\frac{15}{8}+4A\right)\sin^2\chi\right\}\right. \\ &-\left(\frac{189}{32}+\frac{301}{16}\sin^2\chi-\frac{2071}{32}\sin^4\chi+\frac{81}{2}\sin^6\chi\right)r_0^2 \\ &+(1-\sin^2\chi)\left\{-A(6+4\sin^2\chi)+\frac{45}{16}+\frac{15}{8}\sin^2\chi\right. \\ &\left.\left.+\left(-\frac{189}{32}+\frac{645}{32}\sin^2\chi-\frac{81}{2}\sin^4\chi\right)r_0^2\right\}\cos 2t\right] \\ &+O(\epsilon^3) \end{aligned} \tag{16}$$

(see Appendix A). Thus the resonance by the $O(\epsilon^2)$ term occurs around $\cos\chi^{(2)}=\frac{1}{2}$. The corresponding growth rate is found to be

$$\sigma^{(2)}=\epsilon^2\left(\frac{27}{64}\log\frac{8}{\epsilon}-\frac{135}{512}-\frac{63}{128}r_0^2\right)+O(\epsilon^3) \tag{17}$$

(see Appendix B for the details). Since the $O(\epsilon^2)$ perturbation to the basic flow is essentially a strain field, the corresponding growth rate $\sigma^{(2)}$ is related to the growth rate of the elliptical instability[5] as

$$\sigma^{(2)}|_{r_0=0}=\frac{9}{16}\left|A-\frac{15}{32}\right|\epsilon^2. \tag{18}$$

Note that $|A-(15/32)|\epsilon^2$ is the strain rate of $O(\epsilon^2)$ perturbation at the stagnation point $(x,y)=(0,\frac{5}{8}\epsilon+O(\epsilon^2))$.

A similar analysis gives the following growth rate for $\phi=\pi/2$:

$$\begin{aligned} \sigma^{(2)}=&\epsilon^2\left[\left(\frac{27}{64}\log\frac{8}{\epsilon}-\frac{135}{512}-\frac{5}{8}r_0^2\right)^2+\left(\frac{15}{64}r_0^2\right)^2\right]^{1/2} \\ &+O(\epsilon^3), \end{aligned} \tag{19}$$

which takes the same maximum (18) with $\phi=0$ at $r_0=0$. It is worth noting that the maximum of the first-order growth rate for fixed ϕ varies from $(15/256)\epsilon$ for $\phi=0$ to $(165/256)\epsilon$ for $\phi=\pi/2$, while that of the second-order growth rate is the same for $\phi=0$ and $\pi/2$. In fact, in the case of plane pure shear, the growth rate does not depend on ϕ as the potential turns out to be

$$V(t)=4(1-\sin^2\chi)+\varepsilon(1-\sin^2\chi)(6+4\sin^2\chi)\times\cos(2t+\phi)+O(\varepsilon^2),$$

where ε is the rate of strain. Thus the strong dependence of the first-order growth rate on ϕ seems to be a curvature effect.

We should be careful about the effectiveness of the results on the first-order instability. When $\phi\neq 0$ the wavevector is not periodic if we include the higher-order terms; to $O(\epsilon^2)$, the magnitude of the wavevector k is

$$k^2=1+\epsilon(\text{periodic})+\epsilon^2\left[-\frac{21}{16}\sin^2\chi\sin(2\phi)t+(\text{periodic})\right]. \tag{20}$$

Thus k evolves algebraically while $k_\parallel$ is still periodic for $\phi\neq 0,\pi/2$. Since the resonance occurs in a region of χ around $\chi^{(1)}$ of which the width is proportional to ϵr_0, the wavevector fails to satisfy the resonance condition when k becomes smaller than the initial value by $O(\epsilon r_0)$. Therefore the exponential instability saturates around $t=t_f=O(\epsilon^{-1})$, which leads to

$$\log\frac{|\boldsymbol{a}(t_f)|}{|\boldsymbol{a}(0)|}\sim\sigma^{(1)}t_f=O(1).$$

In this case the first-order instability would not be important. For $\phi=\pi/2$, however, k is periodic up to $O(\epsilon^2)$. In fact, there is $O(\epsilon^2)$ difference between the period of the particle motion and that of the wavevector (Appendix B). This implies ϕ may differ from $\pi/2$ by $O(1)$ around $t=O(\epsilon^{-2})$. In other words, the exponential instability saturates around $t=O(\epsilon^{-2})$, which is much larger than t_f for $\phi\neq 0,\pi/2$. Thus the corresponding first-order instability, which has the growth rate (15), would be important since the disturbance grows exponentially for a much longer time.

B. Energy argument

The first-order growth rate can also be obtained by an energy argument as in Waleffe.[5] The inertial wave solution in an unbounded uniformly rotating fluid is known.[17] For the first-order resonance the angular frequency is given by $2\cos\chi=1/2$ at the leading order. Then the disturbance or inertial wave for $\epsilon=0$ is given by

$$\boldsymbol{u}^R=\cos(\boldsymbol{\kappa}\cdot\boldsymbol{r})\left(\hat{\boldsymbol{\kappa}}\times\boldsymbol{v}\cos\frac{t}{2}+\boldsymbol{v}\sin\frac{t}{2}\right),$$

$$\hat{\boldsymbol{\kappa}}=\frac{\boldsymbol{\kappa}}{\kappa}=\begin{pmatrix}\frac{\sqrt{15}}{4}\cos\phi\\ \frac{\sqrt{15}}{4}\sin\phi\\ \frac{1}{4}\end{pmatrix},$$

$$\boldsymbol{v}=\begin{pmatrix}-\sin\phi\cos\beta-\frac{1}{4}\cos\phi\sin\beta\\ \cos\phi\cos\beta-\frac{1}{4}\sin\phi\sin\beta\\ \frac{\sqrt{15}}{4}\sin\beta\end{pmatrix},\quad 0\leqslant\beta<\pi,$$

in a rotating frame.[17] In the inertial frame it becomes

$$\boldsymbol{u}=\cos(\boldsymbol{k}(t)\cdot\boldsymbol{x})\times\begin{pmatrix}\frac{3}{8}\cos\left(\frac{3}{2}t+\phi-\beta\right)-\frac{5}{8}\cos\left(\frac{1}{2}t+\phi+\beta\right)\\ \frac{3}{8}\sin\left(\frac{3}{2}t+\phi-\beta\right)-\frac{5}{8}\sin\left(\frac{1}{2}t+\phi+\beta\right)\\ \frac{\sqrt{15}}{4}\cos\left(\frac{1}{2}t-\beta\right)\end{pmatrix},$$

with $\boldsymbol{k}(t)$ given by $O(1)$ term of (A4). The equation for disturbance energy is

$$\frac{\mathrm{d}}{\mathrm{d}t}\left(\frac{u^2}{2}\right)=-\boldsymbol{u}\cdot[(\boldsymbol{u}\cdot\boldsymbol{\nabla})\boldsymbol{U}]-\boldsymbol{u}\cdot\boldsymbol{\nabla}p.$$

The average of right-hand-side is

$$\overline{-\boldsymbol{u}\cdot[(\boldsymbol{u}\cdot\boldsymbol{\nabla})\boldsymbol{U}]}=\epsilon r_0\frac{15}{256}[5\cos(2\phi+2\beta)-6\cos 2\beta]+O(\epsilon^2)\approx\epsilon r_0\frac{15}{256}\sqrt{61-60\cos 2\phi}\cos(2\beta+\Delta\beta),$$

where $\Delta\beta=-\tan^{-1}[5\sin 2\phi/(6-5\cos 2\phi)]$. The maximum growth rate for fixed ϕ is then evaluated as

$$\sigma=\frac{1}{2}\frac{\overline{-\boldsymbol{u}\cdot[(\boldsymbol{u}\cdot\boldsymbol{\nabla})\boldsymbol{U}]}}{\overline{\frac{u^2}{2}}}\approx\epsilon r_0\frac{15}{256}\sqrt{61-60\cos 2\phi},$$

which coincides with Eq. (14).

C. Numerical results

Equations (2)–(4) are also solved numerically to evaluate the growth rates. We consider the cases $\phi=0$ and $\phi=\pi/2$ since for these values of ϕ the wavevector is periodic up to $O(\epsilon^2)$ so that the growth rates can be obtained with sufficient accuracy. Numerical and analytical results are shown in Figs. 2–4. Figure 2 shows the growth rate obtained numerically by contour lines. Unstable regions are observed around $\chi^{(1)}\approx 0.42\pi$ and $\chi^{(2)}=\pi/3$. Another unstable region with small growth rates is observed around $\chi=0.23\pi$. This is due to the third resonance by the $O(\epsilon)$ term.

Figure 3 compares the numerical and analytical values of the growth rates as functions of r_0. The numerical value is the extremal growth rate for fixed r_0 in Fig. 2. The extrema around $\chi=\chi^{(1)}$ and $\chi^{(2)}$ are identified as first and second orders, respectively. They are in good agreement for $\epsilon=0.02$.

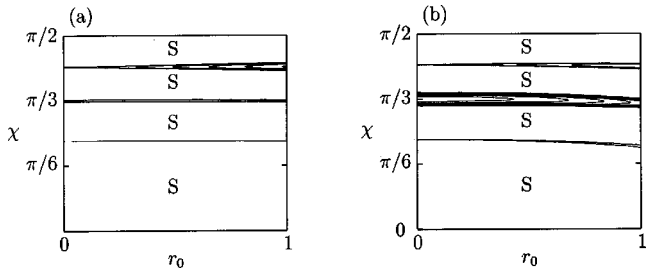

FIG. 2. The contour lines of growth rate. Kelvin's vortex ring. The letter "S" denotes a stable region. (a) $\epsilon=0.1, \phi=\pi/2$, (b) $\epsilon=0.3, \phi=0$.

For $\epsilon=0.1$ the difference between numerical and analytical values is visible for large r_0. This is probably due to a higher-order effect.

Figure 4 compares the maxima of $\sigma^{(1)}$ and $\sigma^{(2)}$ in the core of vortex ring as functions of ϵ. The second-order growth rate for $\phi=\pi/2$ is omitted since it is almost identical with that for $\phi=0$. The numerical and analytical values are in good agreement except that the numerical value of $\sigma^{(1)}$ for $\phi=0$ is much larger than the corresponding analytical value for large ϵ as seen in Fig. 3. According to the analytical results, the first-order instability is stronger than the second-order instability for $0<\epsilon<1$; this range would entirely include the values of ϵ for which the base flow given by the asymptotic expansions are convergent. Moreover even for moderate values of ϵ, the approximation is better than expected within a region of $r\sim O(\epsilon^0)$ since the coefficients of the asymptotic expansions for velocity field decrease exponentially with order of expansions.[18]

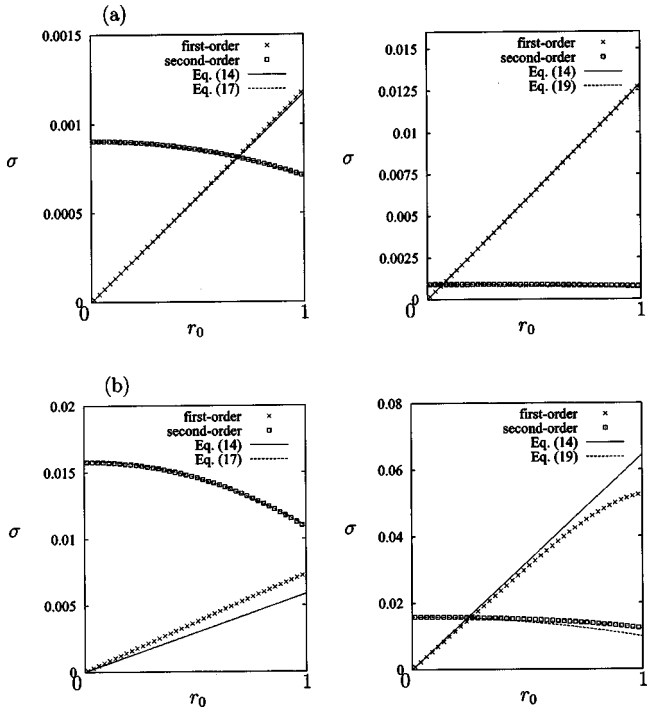

FIG. 3. The first-order and second-order growth rates as functions of r_0. Kelvin's vortex ring. The numerical results are shown by symbols (crosses: first-order, squares: second-order) and the analytical results are shown by lines (solid line: first-order, broken line: second-order). Left: $\phi=0$, right: $\phi=\pi/2$. (a) $\epsilon=0.02$, (b) $\epsilon=0.1$.

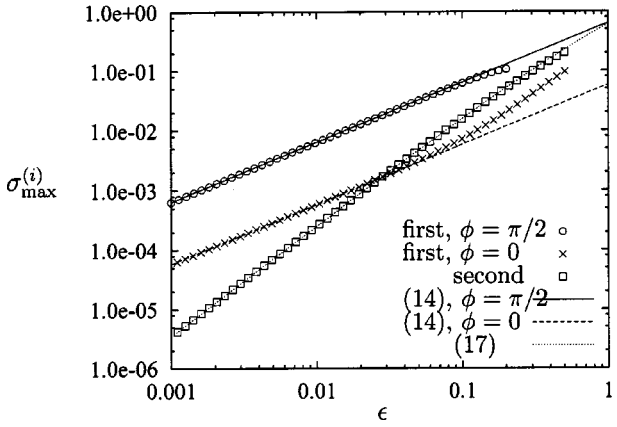

FIG. 4. The maximal growth rates as functions of ϵ. Kelvin's vortex ring. The numerical results are shown by the symbols (circles: first-order, $\phi=\pi/2$, crosses: first-order, $\phi=0$, squares: second-order) and the analytical results are shown by the lines (solid line: first-order, $\phi=\pi/2$, broken line: first-order, $\phi=0$, dotted line: second-order).

IV. STABILITY OF A GAUSSIAN VORTEX RING

A. Basic flow

A general procedure for obtaining the flow field of a thin vortex ring up to $O(\epsilon^2)$ is described in Fukumoto and Moffatt.[19] Here we give a brief summary of their procedure that is required for the following analysis. The leading-order vorticity distribution is assumed to be a Gaussian distribution

$$\omega^{(0)}=\frac{\alpha}{\pi}\exp(-\alpha r^2),$$

where α is a function of time in the presence of viscosity but otherwise is an arbitrary constant. Then the velocity field is given by

$$U_r^{(0)}=0,$$

$$U_\theta^{(0)}=\frac{1}{2\pi r}[1-\exp(-\alpha r^2)],$$

where U_r and U_θ are the radial and the azimuthal components of velocity fields, respectively. Note that the present expressions have some differences in the signs and the definition of θ from the expressions in Fukumoto and Moffatt.[19]

The first-order and second-order fields are obtained by solving the equations of motion expanded by ϵ at each order. The first-order flow field is

$$U_r^{(1)}=-\frac{1}{r}\tilde{\psi}_{11}^{(1)}(r)\cos\theta,$$

$$U_\theta^{(1)}=\left(\frac{d\tilde{\psi}_{11}^{(1)}}{dr}-rU_\theta^{(0)}(r)\right)\sin\theta,$$

where

$$\tilde{\psi}_{11}^{(1)}=\Psi_{11}^{(1)}-c_{11}^{(1)}U_\theta^{(0)},$$

$$\Psi_{11}^{(1)}=U_\theta^{(0)}\left\{\frac{r^2}{2}+\int_0^r\frac{g(r')\mathrm{d}r'}{r'[U_\theta^{(0)}(r')]^2}\right\},$$

$$g(r)=\int_0^r r'[U_\theta^{(0)}(r')]^2\mathrm{d}r'$$

$$=\frac{1}{4\pi^2}\left[\mathrm{E}_1(\alpha r^2)-\frac{1}{2}\mathrm{E}_1(2\alpha r^2)+\log r+\frac{1}{2}\gamma+\frac{1}{2}\ln\frac{\alpha}{2}\right].$$

Here E_1 denotes the exponential integral function and $\gamma=0.577\,215\,664\,9\cdots$ is Euler's constant. The coefficient $c_{11}^{(1)}$ is chosen as

$$c_{11}^{(1)}\approx\frac{1}{4\alpha}2.590\,273\,9=\frac{1}{\alpha}0.648\,184\,8.$$

In fact, $c_{11}^{(1)}$ can be arbitrary because of the freedom in choosing the position of the origin $r=0$; the above choice is the most natural since it keeps the radial position of the origin constant up to $O(\epsilon^3)$ at a finite Reynolds number.

The second-order flow field is given by

$$U_r^{(2)}=\left(\frac{1}{2}\tilde{\psi}_{11}^{(1)}-\frac{2\tilde{\psi}_{21}^{(2)}}{r}\right)\sin 2\theta,$$

$$U_\theta^{(2)}=\left(-\frac{r^2}{2}U_\theta^{(0)}+\frac{r}{2}\frac{\mathrm{d}\tilde{\psi}_{11}^{(1)}}{\mathrm{d}r}-\frac{\mathrm{d}\tilde{\psi}_{21}^{(2)}}{\mathrm{d}r}\right)\cos 2\theta.$$

Here $\tilde{\psi}_{21}^{(2)}$ is obtained by solving the following second-order ordinary differential equation

$$\left(\frac{\mathrm{d}^2}{\mathrm{d}r^2}+\frac{1}{r}\frac{\mathrm{d}}{\mathrm{d}r}-\frac{4}{r^2}-a\right)\tilde{\psi}_{21}^{(2)}$$

$$=\frac{b}{4}(\tilde{\psi}_{11}^{(1)})^2+ra\tilde{\psi}_{11}^{(1)}$$

$$+\frac{1}{2}\left(-rU_\theta^{(0)}+r^2\omega^{(0)}+\frac{\mathrm{d}\tilde{\psi}_{11}^{(1)}}{\mathrm{d}r}-\frac{\tilde{\psi}_{11}^{(1)}}{r}\right),\qquad(21)$$

where a and b are given by

$$a=\frac{1}{U_\theta^{(0)}}\frac{\mathrm{d}\omega^{(0)}}{\mathrm{d}r},\quad b=\frac{1}{U_\theta^{(0)}}\frac{\mathrm{d}a}{\mathrm{d}r},$$

with the boundary conditions

$$\tilde{\psi}_{21}^{(2)}\propto r^2\quad\text{as}\quad r\to 0,$$

$$\tilde{\psi}_{21}^{(2)}\sim\frac{r^2}{4}\left\{\dot{Z}^{(0)}+\frac{1}{8\pi}\left[\log\left(\frac{8}{\epsilon r}\right)-2\right]\right\}+\frac{d^{(1)}}{4}$$

$$\text{as}\quad r\to\infty,$$

where $d^{(1)}=c_{11}^{(1)}/2\pi$. We set $\alpha=1$ in the following. We solve the ordinary differential equation above numerically.

The streamlines and iso-vorticity lines are shown in Fig. 5 for $\epsilon=0.02$ and 0.1. Note that there is a region of weak negative vorticity, which would lead to the centrifugal instability; for $\epsilon=0.02$, it is the upper side of the dashed line corresponding to $\omega_s=0$, and for $\epsilon=0.1$, it is the region between the two dashed lines. This region of negative vorticity is likely an artifact of truncated perturbation expansion. This point is discussed in some detail later.

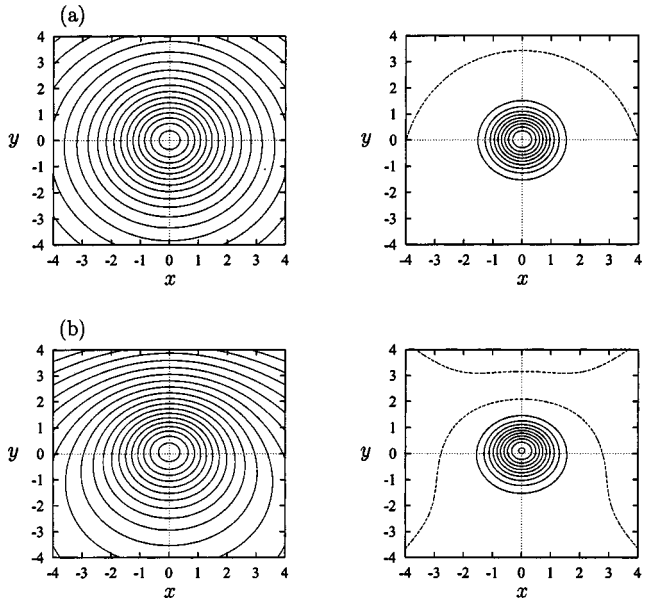

FIG. 5. Streamlines (left) and iso-vorticity lines (right) of a Gaussian vortex ring. The broken lines in the iso-vorticity lines correspond to $\omega_s=0$. (a) $\epsilon=0.02$, (b) $\epsilon=0.1$.

B. Analytical results for the first-order growth rate

The first-order growth rate can be evaluated analytically for a general leading-order flow field. Equations (2) and (3) are solved up to the first order; see Appendix C for the details. The resulting $V(t)$ in the Hill–Schrödinger equation (8) is

$$V(t)=2\omega^{(0)}(r_0)\Omega^{(0)}(r_0)\cos^2\chi$$

$$+\epsilon U_\theta^{(0)}(r_0)F(r_0)\sin(\Omega^{(0)}(r_0)t)+O(\epsilon^2),\qquad(22)$$

where $\Omega^{(0)}=U_\theta^{(0)}/r$ and

$$F(r)=\Omega^{(0)}+2\cos^2\chi\left[(1-4\sin^2\chi)\omega^{(0)}-\Omega^{(0)}\right.$$

$$\left.-\frac{g}{r^2(U_\theta^{(0)})^2}\left\{(2\sin^2\chi-1)\omega^{(0)}+\frac{1}{2}\Omega^{(0)}\right\}\right].$$

The $O(\epsilon)$ term of $V(t)$ causes parametric resonance if $(2\omega^{(0)}\Omega^{(0)}\cos^2\chi)^{1/2}$ is an integral multiple of $\Omega^{(0)}/2$, implying

$$\frac{\omega^{(0)}}{\Omega^{(0)}}=\frac{n^2}{8\cos^2\chi},\quad(n=1,2,\cdots),\qquad(23)$$

among which the growth rate is of $O(\epsilon)$ only for $n=1$. The resonances for Kelvin's case are recovered by substituting the constant value 2 for $\omega^{(0)}/\Omega^{(0)}$. There are contributions to the resonances with $n\geqslant 2$ from higher-order forcing terms with angular frequency $n\Omega^{(0)}$ in $V(t)$. Figure 6 shows the resonance curves in (r,χ) plane for the Gaussian vortex ring. Note that the resonance curve for $n=4$ reduces to the origin and there is no resonance for $n>4$ when the forcing is infinitesimal; there can be resonances for $n>4$ if the forcing is not weak, as observed in the case of two-dimensional multipolar strain.[9]

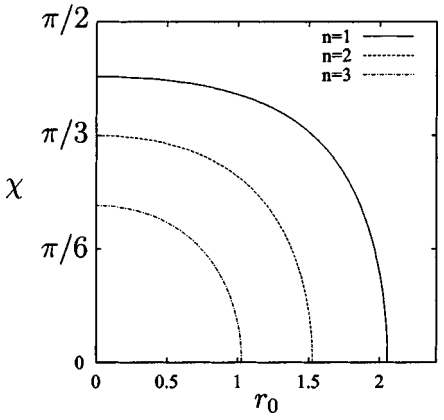

FIG. 6. Resonance curves determined by Eq. (23). Gaussian vortex ring.

By using the resonance condition (23), the first-order growth rate is calculated to be

$$\sigma^{(1)}=\epsilon|U_\theta^{(0)}|\left|\frac{1}{2}\sin^2\chi-\frac{3}{8}-\left(\frac{3}{8}-\frac{1}{4}\sin^2\chi\right)\frac{g}{r_0^2(U_\theta^{(0)})^2}\right| + O(\epsilon^2). \tag{24}$$

Note that r_0 and χ are related through (23) with $n=1$.

C. Numerical results

Equations (2)–(4) are solved numerically using the flow field up to $O(\epsilon^2)$. Figure 7 shows the contour lines of growth rate. Unstable regions are seen around the resonance curves in Fig. 6 with small shifts in r; this is partly because r_0 is simply replaced by $Y_{\max}$, which is the maximum value of $Y(t)$ for each periodic orbit.

Figure 8 compares the numerical and analytical results. As seen in this figure, the first-order growth rate becomes fairly large around $r_0\approx 1.8\sim 2$. For small r_0, it is proportional to $\frac{15}{256}\epsilon U_\theta^{(0)}$, which is essentially the same with Kelvin's case. For larger r_0, however, the change in χ, which is due to the varying frequency ratio $\omega^{(0)}/\Omega^{(0)}$ in the resonance condition (23), has a significant effect of changing the first-order growth rate. The numerical values agree with the analytical value (24) with small shifts in r_0. The behavior of the second-order growth rate, the one for the region emanating from $(r_0,\chi)=(0,\pi/3)$, is rather similar to that of Kelvin's vortex ring; the change in χ has no major effect except for that it gives a cut-off in r_0 around 1.5.

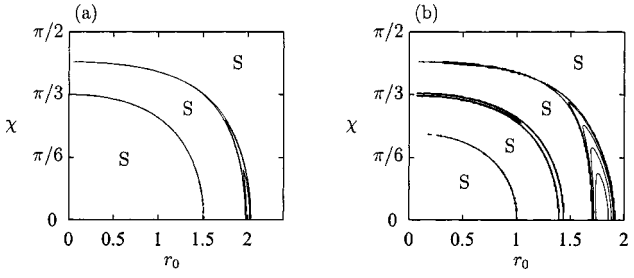

FIG. 7. Contour lines of growth rate. Gaussian vortex ring. (a) $\epsilon=0.02$, (b) $\epsilon=0.1$.

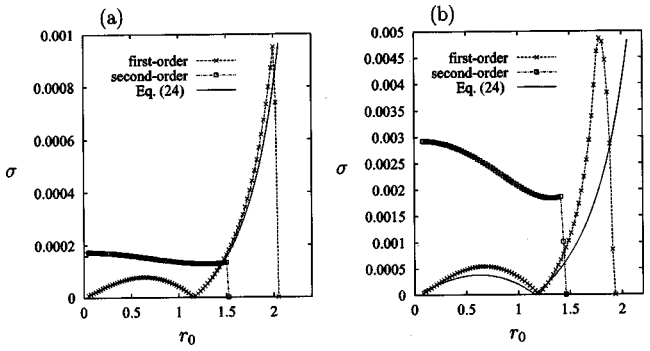

FIG. 8. First-order and second-order growth rates as functions of r_0. Gaussian vortex ring. The numerical results are shown by the symbols (crosses: first-order, squares: second-order) with lines and the analytical value of the first-order growth rate is shown by the solid line. (a) $\epsilon=0.02$, (b) $\epsilon=0.1$.

Finally, the maximum growth rates are plotted against ϵ in Fig. 9. For large values of ϵ the basic flow possesses some amount of error which is due to truncating the perturbation expansions, but the error may not be significant within a region of $r\sim O(\epsilon^0\alpha^{-1/2})$ in the same way as for Kelvin's vortex ring. Numerical results suggest that the first-order growth rate is larger than the second-order one for $\epsilon<\epsilon_c\approx 0.35$, while the analytical line of the first-order growth rate suggests $\epsilon_c\approx 0.2$; therefore, the first-order instability is stronger than or the same order of magnitude with the second-order instability for the values of ϵ for which the base flow is convergent.

D. A remark on the effect of negative vorticity

The asymptotic expansions for the Gaussian core entail nonuniformity in convergence around $r\sim O(\epsilon^{-1/3}\alpha^{-1/2})$. The presence of a region of negative vorticity is traced to this difficulty (see Fig. 5).[19] One may doubt that the results above are related to the centrifugal instability due to the negative vorticity. If this is the case, these results would be wrong since the actual vortex rings are likely to have no region of negative vorticity. However, the unstable region corresponding to the centrifugal instability is found in a separate region

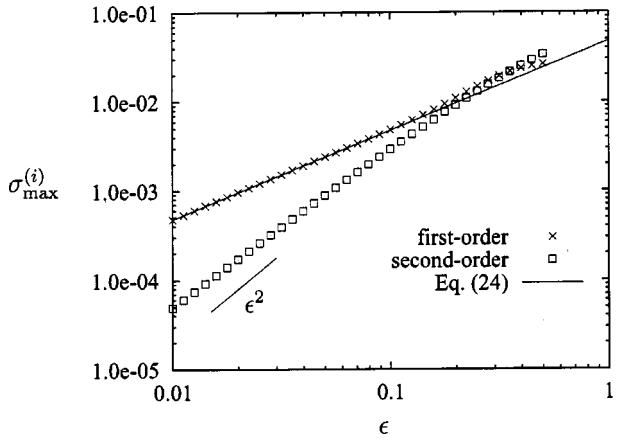

FIG. 9. The maximum growth rates as functions of ϵ. Gaussian vortex ring. The numerical results are shown by symbols (crosses: first-order, squares: second-order) and the analytical value is shown by the solid line for the first-order growth rate.

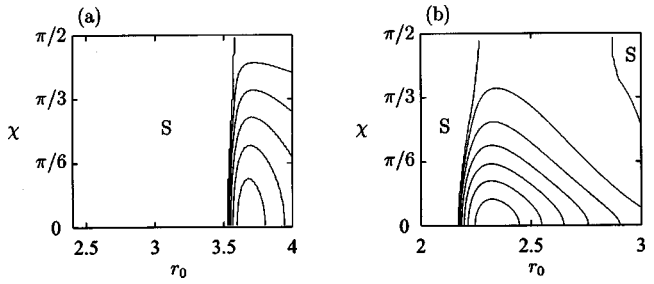

FIG. 10. Contour lines of growth rate for large r_0. Gaussian vortex ring. (a) $\epsilon=0.02$, (b) $\epsilon=0.1$.

in (r,χ)-plane. Figure 10 shows the contour lines of the growth rate for larger values of r_0. For each case there is an unstable region which is irrelevant to the resonance curves. Comparing Fig. 10 with Fig. 5, we see that this unstable region is closely related with the region of negative vorticity. For $\epsilon=0.02$, the vorticity on the y-axis is negative for $y>3.42$; the unstable region is seen in $r_0>3.5$. For $\epsilon=0.1$, the vorticity on the y-axis is negative for $2.08<y<3.16$; the unstable region is seen in $2.2<r_0\leqslant 3.0$, while the orbit is not closed for $r_0\approx Y_{\max}>3.0$. Lifschitz and Hameiri[20] showed that a vortex ring without swirl is unstable on orbits for which the circulation decreases outward by short-wavelength stability analysis; this is a generalization of the classical Rayleigh stability condition. Thus the unstable region seen in Fig. 10 is most likely due to the centrifugal instability. This supports that the unstable regions in Fig. 7, which appear along the resonance curves, are irrelevant to the centrifugal instability.

V. CONCLUDING REMARKS

The linear stability of thin vortex rings is studied in the short wave limit. For both uniform and Gaussian cores the first-order instability is shown to be significant. We should note that there are differences between the two cases. For Kelvin's vortex ring the wavevector which gives the maximum growth rate is non-orthogonal and parallel to the streamline, while the angle χ between the wavevector and the vorticity line is fixed to $\chi^{(1)}\approx 0.42\pi$. For the Gaussian vortex ring, on the other hand, the wavevector is orthogonal to the streamline, while the angle χ which gives the maximum growth rate is 0. Kelvin's vortex ring is special in that the particle motion is isochronous up to $O(\epsilon)$ in the vortex core, which leads to the exponential instability for non-orthogonal wavevector.

In general, inclusion of higher-order terms does not allow the wavevector $\boldsymbol{k}(t)$ to be periodic when $\phi\neq 0$. If so, k evolves algebraically in time and the perturbation goes through amplification only for such a short time as not to grow much as discussed at the end of Sec. III A. Kelvin's vortex ring is an exception in that k is periodic up to $O(\epsilon^2)$ also for $\phi=\pi/2$. The most unstable disturbance occurs in this extreme.

The accuracy of the basic flow of the Gaussian vortex ring may not be sufficient for large value of ϵ. However, the numerical value of the first-order growth rate agrees well with the analytical value for $\epsilon\leqslant 0.15$. Thus there is little doubt about the present results, although the value of ϵ_c, at which second-order instability overtakes the first-order instability, cannot be determined correctly by the present study.

A question would arise how and when we can observe the first-order instability in the experiments. In the experiments by Sullivan *et al.*,[21] the observed unstable waves were supposed to be bending waves. Since it is the second-order effect that destabilizes bending waves, the first-order effect does not seem to have appeared in their experiments. In this regard we mention three points about the case of Gaussian vortex ring. First, the observed unstable waves would depend on the method of introducing initial disturbance. The vorticity is rather small where the first-order growth rate is large; for example, the magnitude of vorticity at $(x,y)\approx(0,1.8)$, where $\sigma^{(1)}$ is maximal for $\epsilon=0.1$, is about 1.7% of the maximum. Thus we should introduce disturbances which have large amplitude in a weak vorticity region in order to observe the first-order instability clearly. Second, viscosity can have a significant effect of stabilization for the first-order effect. In Fig. 8 we see that the first-order growth rate is large in a narrow interval of r_0 near the cut-off, while the second-order growth rate does not vary much below the cut-off; this suggests that the results on the second-order growth rate obtained in the short-wave limit are valid for wavelengths comparable to the core radius, but the results on the first-order growth rate are not. Since the viscous effect enters as $\sigma-\nu k^2$, viscosity can greatly affect the first-order instability if it appears only for short waves. Finally, nonlinearity is neglected in the present analysis. We should take account of nonlinear effect in order to deal with the large-amplitude waves observed in Sullivan *et al.*[21]

It is of interest to study how the present results by short-wavelength analysis are related with those by normal-mode stability analysis. For Kelvin's ring, the growth rate $\sigma^{(1)}=(15\epsilon/256)$ for $\phi=0$ is realizable by parametric resonance between the axisymmetric and the bending modes.[6] Instability with a larger growth rate occurs for interaction of higher modes, which will be reported elsewhere. For the Gaussian ring, the method explored by Bayly[22] would give a clue. Applying this method with required modification, the quantity $C(\psi)$ is shown to be positive for the streamline of the maximal growth rate; it strongly suggests that there is a localized normal mode which corresponds to the maximal growth rate found by the present short-wavelength analysis (see Appendix D for the details).

ACKNOWLEDGMENTS

Y.H. was partially supported by an overseas research program of MEXT, Japan. We were also supported in part by a Grant-in-Aid for Scientific Research from the Japan Society for the Promotion of Science.

APPENDIX A: SOLUTIONS TO EQS. (2) AND (3) FOR KELVIN'S VORTEX RING

Here we describe some details of solving Eqs. (2) and (3) for Kelvin's vortex ring. Since the basic flow is axisymmetric and the azimuthal component of velocity (swirl) is

zero, the particle path lies on a plane $s=\text{const}$. We can take $s=0$ without loss of generality. The basic flow in the core is assumed to be the Rankine vortex at $O(1)$. Then the steady Euler equation is solved by asymptotic expansion in ϵ to give

$$U_r=\epsilon\frac{5}{8}(1-r^2)\cos\theta+\epsilon^2\left(Ar+\frac{r^3}{8}\right)\sin 2\theta+O(\epsilon^3),$$

$$U_\theta=r+\epsilon\left(-\frac{5}{8}+\frac{7}{8}r^2\right)\sin\theta+\epsilon^2\left(Ar+\frac{r^3}{16}\right)\cos 2\theta+O(\epsilon^3),$$

$$U_s=0,$$

in (r,θ,s) coordinate system shown in Fig. 1.[1] We would like to work in the local Cartesian coordinate system (x,y,z). Using the relations

$$x=r\cos\theta,\quad \epsilon y=(1+\epsilon r\sin\theta)\cos(\epsilon s)-1,$$

$$\epsilon z=(1+\epsilon r\sin\theta)\sin(\epsilon s),$$

$$\boldsymbol{e}_r=\cos\theta\boldsymbol{e}_x+\sin\theta\cos(\epsilon s)\boldsymbol{e}_y+\sin\theta\sin(\epsilon s)\boldsymbol{e}_z,$$

$$\boldsymbol{e}_\theta=-\sin\theta\boldsymbol{e}_x+\cos\theta\cos(\epsilon s)\boldsymbol{e}_y+\cos\theta\sin(\epsilon s)\boldsymbol{e}_z,$$

$$\boldsymbol{e}_s=-\sin(\epsilon s)\boldsymbol{e}_y+\cos(\epsilon s)\boldsymbol{e}_z,$$

with $\boldsymbol{e}_i$ being the unit vector in the ith direction, we obtain Eq. (11) in this coordinate system after straightforward calculation. Note that this expression is valid for $|z|\leqslant O(1)$ though we require an expression valid just around the plane $z=0$, which is identical with $s=0$. The matrix $\mathcal{L}$ is

$$\mathcal{L}=\begin{pmatrix}0&-1&0\\1&0&0\\0&0&0\end{pmatrix}+\epsilon\begin{pmatrix}-\frac{5}{4}x&-\frac{7}{4}y&-z\\\frac{1}{4}y&\frac{1}{4}x&0\\z&0&x\end{pmatrix}+\epsilon^2\begin{pmatrix}\frac{3}{8}xy&A+\frac{3}{16}x^2+\frac{3}{16}y^2-\frac{3}{8}z^2&-\frac{3}{4}yz\\A+\frac{3}{16}x^2+\frac{3}{16}y^2-\frac{3}{8}z^2&\frac{3}{8}xy&-\frac{3}{4}xz\\-\frac{3}{4}yz&-\frac{3}{4}xz&-\frac{3}{4}xy\end{pmatrix}+O(\epsilon^3). \tag{A1}$$

First, we should know the particle motion $\boldsymbol{X}(t)$ up to $O(\epsilon)$; since the matrix $\mathcal{L}$ does not depend on $\boldsymbol{x}$ at the leading order, $O(\epsilon^2)$ precision is not required for $\boldsymbol{X}(t)$. Equation (2) is solved as

$$\boldsymbol{X}(t)=\begin{pmatrix}r_0\cos\Omega t\\r_0\sin\Omega t\\0\end{pmatrix}+\epsilon\begin{pmatrix}\frac{r_0^2}{8}\sin 2\Omega t\\\frac{5}{8}-\frac{3r_0^2}{4}-\frac{r_0^2}{8}\cos 2\Omega t\\0\end{pmatrix}+O(\epsilon^2), \tag{A2}$$

for an appropriate initial condition, where $\Omega=1$ up to the first order.

Next, substituting the particle motion above to Eq. (3), we obtain the following equations for local wavevector:

$$\frac{\mathrm{d}\boldsymbol{k}}{\mathrm{d}t}=\begin{pmatrix}-k_y\\k_x\\0\end{pmatrix}+\epsilon\begin{pmatrix}\frac{5r_0}{4}\cos\Omega t\ \ k_x-\frac{r_0}{4}\sin\Omega t\ \ k_y\\\frac{7r_0}{4}\sin\Omega t\ \ k_x-\frac{r_0}{4}\cos\Omega t\ \ k_y\\-r_0\cos\Omega t\ \ k_z\end{pmatrix}+\epsilon^2\begin{pmatrix}-\frac{r_0^2}{32}\sin 2\Omega t\ \ k_x+\left(-A-\frac{5}{32}+\frac{r_0^2}{32}\cos 2\Omega t\right)k_y\\\left(-A+\frac{35}{32}-\frac{3r_0^2}{2}-\frac{7r_0^2}{32}\cos 2\Omega t\right)k_x-\frac{7r_0^2}{32}\sin 2\Omega t\ \ k_y\\\frac{r_0^2}{4}\sin 2\Omega t\ \ k_z\end{pmatrix}+O(\epsilon^3). \tag{A3}$$

For the initial condition $\boldsymbol{k}(0)=(\sin\chi\cos\phi,\sin\chi\sin\phi,\cos\chi)^T+O(\epsilon)$, the solution reads

$$\boldsymbol{k}(t)=\begin{pmatrix}\sin\chi\cos(\Omega t+\phi)\\\sin\chi\sin(\Omega t+\phi)\\\cos\chi\end{pmatrix}+\epsilon\begin{pmatrix}r_0\sin\chi[\sin\phi+\frac{3}{4}\sin(2\Omega t+\phi)]\\r_0\sin\chi[\frac{1}{2}\cos\phi-\frac{3}{4}\cos(2\Omega t+\phi)]\\-r_0\cos\chi\sin\Omega t\end{pmatrix}$$
$$+\epsilon^2\begin{pmatrix}r_0^2\sin\chi[-\frac{9}{32}\cos(3\Omega t+\phi)-\frac{21}{16}\sin\phi t\cos(\Omega t)]\\r_0^2\sin\chi[-\frac{9}{32}\sin(3\Omega t+\phi)-\frac{21}{16}\sin\phi t\sin(\Omega t)]+B\sin\chi\sin(\Omega t+\phi)\\r_0^2\cos\chi[\frac{1}{4}-\frac{3}{8}\cos(2\Omega t+\phi)]\end{pmatrix}+O(\epsilon^3), \tag{A4}$$

where $B=-A+\frac{15}{32}-(7r_0^2/16)$ and the angular velocity is corrected as

$$\Omega=1+\epsilon^2\left(\frac{5}{8}-\frac{21}{32}r_0^2\right), \tag{A5}$$

because of secular terms. The $O(\epsilon^2)$ terms of $\boldsymbol{k}$ have aperiodic terms $t\cos\Omega t$ and $t\sin\Omega t$. For $\phi=0$ these terms vanish. For $\phi=\pi/2$ these terms can be included in the $O(1)$ terms by correcting the angular velocity as

$$\Omega'=\Omega+\epsilon^2\frac{21r_0^2}{16}, \tag{A6}$$

so that the wavevector $\boldsymbol{k}$ is periodic up to $O(\epsilon^2)$. For $\phi\neq 0,\pi/2$, $\boldsymbol{k}$ is not periodic up to $O(\epsilon^2)$.

Finally, by substituting the solutions above into Eq. (9), we obtain Eq. (13) for general ϕ and Eq. (16) for $\phi=0$.

APPENDIX B: GROWTH RATES OF UNSTABLE SOLUTIONS TO HILL–SCHRÖDINGER EQUATION BY MATHIEU'S METHOD

Here we apply Mathieu's method to the Hill–Schrödinger equation (8) to obtain the growth rate. The potential $V(t)$ is expressed as

$$V(t)=\sum_{m=-2}^{2}a_m e^{\mathrm{i}m\Omega t}+O(\epsilon^3),$$

$$a_0=A_0+\epsilon^2 B_0,\quad a_{\pm1}=\epsilon A_{\pm1},\quad a_{\pm2}=\epsilon^2 A_{\pm2},$$

$$A_{-m}^{*}=A_m,$$

in the cases under consideration. Let us consider a solution of the type

$$q(t)=e^{\mu t}\sum_{n=-\infty}^{\infty}b_{n/2}\exp\left(\mathrm{i}\frac{n}{2}\Omega t\right). \tag{B1}$$

Substituting the above expressions to Eq. (8) we obtain the following set of linear equations for b_n and μ:

$$\left(\mu+\mathrm{i}\frac{n}{2}\Omega\right)^2 b_{n/2}+\sum_{m=-2}^{2}a_m b_{n/2-m}=0. \tag{B2}$$

We expand χ, μ and $b_{n/2}$ as

$$\chi=\chi^{(0)}+\epsilon\chi^{(1)}+\epsilon^2\chi^{(2)}+O(\epsilon^3),$$

$$\mu=\mu^{(0)}+\epsilon\mu^{(1)}+\epsilon^2\mu^{(2)}+O(\epsilon^3),$$

$$b_{n/2}=b_{n/2}^{(0)}+\epsilon b_{n/2}^{(1)}+\epsilon^2 b_{n/2}^{(2)}+O(\epsilon^3).$$

The coefficients A_m and B_0 are also expanded as

$$\begin{aligned}A_m&=A_m(\chi)\\&=A_m(\chi^{(0)})+\epsilon\left.\frac{\partial A_m}{\partial\chi}\right|_{\chi^{(0)}}\chi^{(1)}+\epsilon^2\left[\left.\frac{\partial A_m}{\partial\chi}\right|_{\chi^{(0)}}\chi^{(2)}\right.\\&\quad\left.+\frac{1}{2}\left.\frac{\partial^2 A_m}{\partial\chi^2}\right|_{\chi^{(0)}}(\chi^{(1)})^2\right]+O(\epsilon^3)\\&=A_m^{(0)}+\epsilon A_m^{(1)}+\epsilon^2 A_m^{(2)}+O(\epsilon^3).\end{aligned}$$

Then Eq. (B2) becomes

$$\begin{aligned}&\left[\left(\mu^{(0)}+\mathrm{i}\frac{n}{2}\Omega+\epsilon\mu^{(1)}+\epsilon^2\mu^{(2)}\right)^2\right.\\&\quad\left.+A_0^{(0)}+\epsilon A_0^{(1)}+\epsilon^2(B_0^{(0)}+A_0^{(2)})\right](b_{n/2}^{(0)}+\epsilon b_{n/2}^{(1)}+\epsilon^2 b_{n/2}^{(2)})\\&\quad+\epsilon(A_1^{(0)}+\epsilon A_1^{(1)})(b_{n/2-1}^{(0)}+\epsilon b_{n/2-1}^{(1)})\\&\quad+\epsilon(A_{-1}^{(0)}+\epsilon A_{-1}^{(1)})(b_{n/2+1}^{(0)}+\epsilon b_{n/2+1}^{(1)})\\&\quad+\epsilon^2 A_2^{(0)}b_{n12-2}^{(0)}+\epsilon^2 A_{-2}^{(0)}b_{n/2+2}^{(0)}+O(\epsilon^3)=0.\end{aligned} \tag{B3}$$

At $O(1)$, we obtain

$$\left[\left(\mu^{(0)}+\mathrm{i}\frac{n}{2}\Omega\right)^2+A_0^{(0)}\right]b_{n/2}^{(0)}=0. \tag{B4}$$

Without loss of generality, we obtain

$$\mu^{(0)}=0,\quad A_0^{(0)}=N^2\Omega^2/4,\quad b_{\pm N/2}^{(0)}\neq 0,$$

$$b_{n/2}^{(0)}=0\ \text{ for }\ n\neq N,$$

in order to have a non-trivial solution.

1. $N=1$

The most important resonance by the first-order term of $V(t)$ occurs when $N=1$. In this case, the $O(\epsilon)$ relation of Eq. (B3) becomes

$$\begin{aligned}&\frac{1-n^2}{4}\Omega^2 b_{n/2}^{(1)}+(\mathrm{i}n\Omega\mu^{(1)}+A_0^{(1)})b_{n/2}^{(0)}+A_1^{(0)}b_{n/2-1}^{(0)}\\&\quad+A_{-1}^{(0)}b_{n/2+1}^{(0)}=0.\end{aligned} \tag{B5}$$

From the above equations for $n=\pm1$ we obtain

$$\Omega^2(\mu^{(1)})^2=|A_1^{(0)}|^2-(A_0^{(1)})^2,\quad \mathrm{Im}\,A_0^{(1)}=0.$$

Thus the maximum of $\mu^{(1)}$ is attained at $A_0^{(1)}=0$, which implies $\chi^{(1)}=0$ and hence $A_n^{(1)}=0$; the maximum is

$$\mu^{(1)}=\frac{|A_1^{(0)}|}{\Omega},$$

and we have

$$b_{1/2}^{(0)}=\mathrm{i}\frac{A_1^{(0)}}{|A_1^{(0)}|}b_{-1/2}^{(0)}. \tag{B6}$$

Equation (B5) further gives

$$b_{\pm 3/2}=\frac{A_{\pm 1}^{(0)}b_{\pm 1/2}^{(0)}}{2\Omega^2},\quad b_{n/2}=0 \ \text{ for } |n|\neq 1,3.$$

The $O(\epsilon^2)$ relation of Eq. (B3) is now

$$\frac{1-n^2}{4}\Omega^2 b_{n/2}^{(2)}+in\Omega\mu^{(1)}b_{n/2}^{(1)}+[in\Omega\mu^{(2)}+(\mu^{(1)})^2+B_0^{(0)}+A_0^{(2)}]b_{n/2}^{(0)}+A_1^{(0)}b_{n/2-1}^{(1)}+A_{-1}^{(0)}b_{n/2+1}^{(1)}+A_2^{(0)}b_{n/2-2}^{(0)}+A_{-2}^{(0)}b_{n/2+2}^{(0)}=0. \tag{B7}$$

From the above equations for $n=\pm 1$ and Eq. (B6) we have

$$\frac{\dfrac{|A_1^{(0)}|^2}{\Omega^2}+B_0^{(0)}+A_0^{(2)}-i\Omega\mu^{(2)}}{\dfrac{|A_1^{(0)}|^2}{\Omega^2}+B_0^{(0)}+A_0^{(2)}+i\Omega\mu^{(2)}}=\frac{b_{1/2}^{(0)}}{b_{-1/2}^{(0)}}\cdot\frac{-A_{-1}^{(0)}b_{1/2}^{(1)}+i|A_{-1}^{(0)}|b_{-1/2}^{(1)}}{-i|A_1^{(0)}|b_{1/2}^{(1)}-A_1^{(0)}b_{-1/2}^{(1)}}=1, \tag{B8}$$

which implies $\mu^{(2)}=0$. To summarize,

$$\sigma^{(1)}=\mu=\epsilon\frac{|A_1^{(0)}|}{\Omega}+O(\epsilon^3). \tag{B9}$$

2. $N=2$

The most important resonance by the second-order term of $V(t)$ occurs when $N=2$. In this case, the $O(\epsilon)$ relation of Eq. (B3) becomes

$$\frac{4-n^2}{4}\Omega^2 b_{n/2}^{(1)}+(in\Omega\mu^{(1)}+A_0^{(1)})b_{n/2}^{(0)}+A_1^{(0)}b_{n/2-1}^{(0)}+A_{-1}^{(0)}b_{n/2+1}^{(0)}=0. \tag{B10}$$

From the above equations for $n=\pm 2$ we obtain

$$\mu^{(1)}=A_0^{(1)}=0.$$

Hence $\chi^{(1)}=0$ and $A_m^{(1)}=0$. Equation (B10) further gives

$$b_0^{(1)}=-A_1^{(0)}b_{-1}^{(0)}-A_{-1}^{(0)}b_1^{(0)},\quad b_{\pm 2}^{(1)}=\frac{A_{\pm 1}^{(0)}b_{\pm 1}^{(0)}}{3},$$

$$b_{n/2}=0 \ \text{ for } |n|\neq 0,2,4.$$

The $O(\epsilon^2)$ relation of Eq. (B3) is now

$$\frac{4-n^2}{4}\Omega^2 b_{n/2}^{(2)}+[in\Omega\mu^{(2)}+B_0^{(0)}+A_0^{(2)}]b_{n/2}^{(0)}+A_1^{(0)}b_{n/2-1}^{(1)}+A_{-1}^{(0)}b_{n/2+1}^{(1)}+A_2^{(0)}b_{n/2-2}^{(0)}+A_{-2}^{(0)}b_{n/2+2}^{(0)}=0. \tag{B11}$$

From the above equations for $n=\pm 2$ we obtain

$$4\Omega^2(\mu^{(2)})^2+\left(B_0^{(0)}+A_0^{(2)}-\frac{2}{3}|A_1^{(0)}|\right)^2=|A_2^{(0)}-(A_1^{(0)})^2|^2.$$

For Kelvin's ring, it is possible to choose $\chi^{(2)}$ so that $A_0^{(2)}=-B_0^{(0)}+2|A_1^{(0)}|^2/3$ since $(\partial A_0/\partial\chi)|_{\chi^{(0)}}\neq 0$. Thus the maximal growth rate is

$$\sigma^{(2)}=\mu=\epsilon^2\frac{1}{2\Omega}|A_2^{(0)}-(A_1^{(0)})^2|+O(\epsilon^3).$$

APPENDIX C: SOLUTIONS TO EQS. (2) AND (3) FOR A GENERAL LEADING-ORDER BASIC FLOW UP TO THE FIRST ORDER

Here we describe solutions to Eqs. (2) and (3) for a general leading-order basic flow, which are required for obtaining the first-order growth rate (24). We use the coordinate system (r,θ,s) since singularity does not arise up to the first order.

The matrix $\mathcal{L}$ is represented as

$$\mathcal{L}=\begin{pmatrix}\mathcal{L}_\perp & 0\\ 0^T & \mathcal{L}_\parallel\end{pmatrix}, \tag{C1}$$

$$\mathcal{L}_\perp=\begin{pmatrix}0 & -\dfrac{U_\theta^{(0)}}{r}\\ \dfrac{dU_\theta^{(0)}}{dr} & 0\end{pmatrix}+\epsilon\begin{pmatrix}\dfrac{d\tilde{U}_r^{(1)}}{dr}\cos\theta & -\dfrac{1}{r}(\tilde{U}_r^{(1)}+\tilde{U}_\theta^{(1)})\sin\theta\\ \dfrac{d\tilde{U}_\theta^{(1)}}{dr}\sin\theta & \dfrac{1}{r}(\tilde{U}_r^{(1)}+\tilde{U}_\theta^{(1)})\cos\theta\end{pmatrix}+O(\epsilon^2), \tag{C2}$$

$$\mathcal{L}_\parallel=\epsilon U_\theta^{(0)}\cos\theta+O(\epsilon^2), \tag{C3}$$

where

$$\tilde{U}_r^{(1)}(r)=-\frac{1}{r}\tilde{\psi}_{11}^{(1)}(r),\quad \tilde{U}_\theta^{(1)}(r)=\frac{d\tilde{\psi}_{11}^{(1)}}{dr}+rU_\theta^{(0)}(r).$$

First, we solve the particle motion. Equation (2) is written as

$$\frac{dR}{dt}=U_r,\quad R\frac{d\Theta}{dt}=U_\theta.$$

The solution is

$$R(t)=r_0+\epsilon\frac{\tilde{U}_r^{(1)}}{\Omega^{(0)}}\sin(\Omega^{(0)}t)+O(\epsilon^2),$$

$$\Theta(t)=\Omega^{(0)}t+O(\epsilon).$$

Since the matrix $\mathcal{L}$ does not depend on θ at the leading order, the $O(\epsilon)$ term of Θ is not required.

Next, we solve the wavevector equation (3). It is written as

$$\left[\frac{d}{dt}+\begin{pmatrix}0 & -\Omega\\ \Omega & 0\end{pmatrix}\right]\boldsymbol{k}_\perp=-\mathcal{L}_\perp^T\boldsymbol{k}_\perp,\quad \frac{dk_\parallel}{dt}=-\mathcal{L}_\parallel k_\parallel,$$

in the present coordinate system. Substituting $R(t)$ and $\Theta(t)$ to the above equations, the wavevector is found to be

$$\boldsymbol{k}(t)=\begin{pmatrix}\sin\chi\\0\\\cos\chi\end{pmatrix}+\epsilon\begin{pmatrix}-\dfrac{\sin\chi}{\Omega^{(0)}}\left[\dfrac{d\tilde{U}_r^{(1)}}{dr}+\left(\Omega^{(0)}-\dfrac{dU_\theta^{(0)}}{dr}\right)\dfrac{\tilde{U}_r^{(1)}}{\Omega^{(0)}r_0}\right]\sin(\Omega^{(0)}t)\\-\dfrac{\sin\chi\,\tilde{U}_r^{(1)}}{\Omega^{(0)}r_0}\cos(\Omega^{(0)}t)\\-r_0\cos\chi\sin(\Omega^{(0)}t)\end{pmatrix}+O(\epsilon^2),$$

for the initial condition $\boldsymbol{k}(0)=(\sin\chi,0,\cos\chi)^T+O(\epsilon)$. The functions in $O(\epsilon)$ terms are evaluated at $r=r_0$.

Finally, by substituting the solutions above into Eq. (9) we obtain Eq. (22).

APPENDIX D: ON THE EXISTENCE OF NORMAL MODES

Here we discuss the existence of normal modes which correspond to the first-order instability for the Gaussian vortex ring. We proceed in the same way as in Bayly,[22] who discussed the existence of localized unstable modes for centrifugal-type instability. The key issue is to calculate $C(\psi)$ defined below by Eq. (D5); since $C(\psi)$ should be modified for the present case, we briefly describe its derivation.

For the Gaussian ring, the first-order instability has the maximum growth rate at $\chi=0$, which implies the wavevector is in the direction of s-axis. This suggests that the corresponding unstable mode can be constructed in the similar way with Bayly.[22] Let us consider a normal-mode perturbation

$$\boldsymbol{u}=(\tilde{\boldsymbol{u}}(r,\theta),\tilde{p}(r,\theta))\exp(\mathrm{i}ks+St)+\text{c.c.},$$

where $k\gg1$. We expand $\tilde{\boldsymbol{u}}$ as

$$\tilde{\boldsymbol{u}}=\sum_{i=1}^{3}\tilde{u}_i\boldsymbol{f}_i,$$

where $\boldsymbol{f}_i$ is the Floquet characteristic vector field.[22] The equation for the perturbation reduces to

$$[S-\Sigma(\psi)+\boldsymbol{U}\cdot\boldsymbol{\nabla}_\perp]\tilde{u}_1=-\boldsymbol{f}_1^\dagger\cdot\boldsymbol{\nabla}_\perp\tilde{p},\tag{D1}$$

$$[S+\Sigma(\psi)+\boldsymbol{U}\cdot\boldsymbol{\nabla}_\perp]\tilde{u}_2=-\boldsymbol{f}_2^\dagger\cdot\boldsymbol{\nabla}_\perp\tilde{p},\tag{D2}$$

$$(S+\boldsymbol{U}\cdot\boldsymbol{\nabla}_\perp)\tilde{u}_3=-\frac{\mathrm{i}k}{1+\epsilon r\sin\theta}\tilde{p},\tag{D3}$$

$$(\boldsymbol{\nabla}_\perp+\epsilon\boldsymbol{e}_y)\cdot(\tilde{u}_1\boldsymbol{f}_1+\tilde{u}_2\boldsymbol{f}_2)+\frac{\mathrm{i}k}{1+\epsilon r\sin\theta}\tilde{u}_3=0,\tag{D4}$$

where $\Sigma(\psi)$ is the positive Floquet exponent corresponding to $\boldsymbol{f}_1$, $\boldsymbol{\nabla}_\perp=\boldsymbol{e}_r\partial_r+r^{-1}\boldsymbol{e}_\theta\partial_\theta$ and $\boldsymbol{f}_i^\dagger$ is the adjoint Floquet characteristic vector field. Note that owing to the curvature effect there are some differences from the equations derived by Bayly.[22] We assume the same scaling in k with Bayly[22]

$$\tilde{u}_1=U_1,\quad \tilde{u}_2=k^{-1}U_2,\quad \tilde{u}_3=k^{-1/2}U_3,$$
$$\tilde{p}=k^{-3/2}P,\quad S=\Sigma(\psi_0)-k^{-1}S_1,$$

with corrections of higher order in k^{-1}. The solution above is localized within a region of width $O(k^{-1/2})$ around the streamline $\psi=\psi_0$, for which the growth rate reaches the maximum. Introducing the scaled streamline coordinate $\eta=k^{1/2}(\psi-\psi_0)$, Eq. (D4) reduces to

$$(\boldsymbol{f}_1\cdot\boldsymbol{\nabla}_\perp)\frac{\partial U_1}{\partial\eta}=-\frac{\mathrm{i}}{1+\epsilon r\sin\theta}U_3,$$

at the leading order. This together with Eq. (D3) gives

$$P=-(1+\epsilon r\sin\theta)[\Sigma(\psi_0)+\boldsymbol{U}\cdot\boldsymbol{\nabla}_\perp]\left[(\boldsymbol{f}_1\cdot\boldsymbol{\nabla}_\perp)\frac{\partial U_1}{\partial\eta}\right].$$

Substituting P into Eq. (D1), we obtain

$$\left[-\frac{1}{2}\Sigma''(\psi_0)\eta^2-S_1\right]U_1=(1+\epsilon r\sin\theta)(\boldsymbol{f}_1^\dagger\cdot\boldsymbol{\nabla}_\perp\psi)[\Sigma(\psi_0)+\boldsymbol{U}\cdot\boldsymbol{\nabla}_\perp]\times(1+\epsilon r\sin\theta)(\boldsymbol{f}_1\cdot\boldsymbol{\nabla}_\perp\psi)\frac{\partial^2U_1}{\partial\eta^2},$$

with $\boldsymbol{U}\cdot\boldsymbol{\nabla}_\perp U_1=0$. Averaging over the streamline $\psi=\psi_0$, we obtain

$$\left[-\frac{1}{2}\Sigma''(\psi_0)\eta^2-S_1\right]\overline{U}_1(\eta)=C(\psi_0)\frac{\partial^2}{\partial\eta^2}\overline{U}_1(\eta),$$

where

$$C(\psi)=\frac{1}{T(\psi)}\int_0^{T(\psi)}d\tau\{(1+\epsilon r\sin\theta)(\boldsymbol{f}_1^\dagger\cdot\boldsymbol{\nabla}_\perp\psi)\times[\Sigma(\psi_0)+\boldsymbol{U}\cdot\boldsymbol{\nabla}_\perp](1+\epsilon r\sin\theta)(\boldsymbol{f}_1\cdot\boldsymbol{\nabla}_\perp\psi)\}_{\boldsymbol{X}(\tau)},\tag{D5}$$

which coincides with the expression in Bayly[22] if $\epsilon=0$.

We calculate $C(\psi)$ up to $O(\epsilon)$. The components of Floquet characteristic vector fields $\boldsymbol{f}_1$ and $\boldsymbol{f}_2$ turn out to be

$$f_{1r}=\sin\left(\frac{1}{2}\Omega^{(0)}\tau\right)-\epsilon\frac{H_+}{2[\Omega^{(0)}]^2}\cos\left(\frac{3}{2}\Omega^{(0)}\tau\right),$$

$$f_{1\theta}=\frac{1}{4}\cos\left(\frac{1}{2}\Omega^{(0)}\tau\right)+\epsilon\left(\frac{3H_+}{8[\Omega^{(0)}]^2}-\frac{G_{1+}}{2\Omega^{(0)}}\right)\sin\left(\frac{3}{2}\Omega^{(0)}\tau\right)+\epsilon\left(\frac{H_-}{4[\Omega^{(0)}]^2}-\frac{G_{1-}}{2\Omega^{(0)}}\right)\sin\left(\frac{1}{2}\Omega^{(0)}\tau\right),$$

$$f_{2r}=\cos\left(\frac{1}{2}\Omega^{(0)}\tau\right)+\epsilon\frac{H_+}{2[\Omega^{(0)}]^2}\sin\left(\frac{3}{2}\Omega^{(0)}\tau\right),$$

$$f_{2\theta}=-\frac{1}{4}\sin\left(\frac{1}{2}\Omega^{(0)}\tau\right)$$
$$-\epsilon\left(\frac{3H_+}{8[\Omega^{(0)}]^2}-\frac{G_{1+}}{2\Omega^{(0)}}\right)\cos\left(\frac{3}{2}\Omega^{(0)}\tau\right)$$
$$-\epsilon\left(\frac{H_-}{4[\Omega^{(0)}]^2}-\frac{G_{1-}}{2\Omega^{(0)}}\right)\cos\left(\frac{1}{2}\Omega^{(0)}\tau\right),$$

$$f_{1s}=f_{2s}=0,$$

as functions of τ on the streamline $\psi=\psi_0$. Here

$$G_{1\pm}=\frac{\Omega_f}{4\Omega^{(0)}}\left(\frac{2\tilde{U}_r^{(1)}}{r_0\Omega^{(0)}}\frac{dU_\theta^{(0)}}{dr}-\frac{\tilde{U}_r^{(1)}}{r_0}+\frac{2\tilde{U}_\theta^{(1)}}{r_0}\right)$$
$$\mp\frac{1}{2}\frac{d\tilde{U}_r^{(1)}}{dr},$$

$$G_{2\pm}=\pm\left(\frac{\tilde{U}_r^{(1)}}{2\Omega^{(0)}}\frac{d^2U_\theta^{(0)}}{dr^2}+\frac{\tilde{U}_r^{(1)}}{2r_0\Omega^{(0)}}\frac{dU_\theta^{(0)}}{dr}-\frac{\tilde{U}_r^{(1)}}{2r_0}+\frac{\tilde{U}_\theta^{(1)}}{2r_0}\right.$$
$$\left.+\frac{1}{2}\frac{d\tilde{U}_\theta^{(1)}}{dr}\right)-\frac{\Omega_f}{4r_0\Omega^{(0)}}(\tilde{U}_r^{(1)}+\tilde{U}_\theta^{(1)}),$$

$$H_\pm=(\Omega^{(0)}\pm\Omega_f)G_{1\pm}+2\Omega^{(0)}G_{2\pm},$$

$$\tilde{U}_r^{(1)}(r)=U_r^{(1)}/\cos\theta,\quad \tilde{U}_\theta^{(1)}(r)=U_\theta^{(1)}/\sin\theta,$$

where all functions of r in the above are evaluated at $r=r_0$ and $\Omega_f=(2\Omega^{(0)}\omega^{(0)})^{1/2}=\Omega^{(0)}/2$ for the present case. Using these expressions, we obtain

$$C(\psi_0)=\epsilon[U_\theta^{(0)}]^3\left[\frac{37}{512}-\frac{41c_{11}^{(1)}}{256r_0^2}-\frac{5g(r_0)}{128r_0^2(U_\theta^{(0)})^2}\right.$$
$$\left.+\frac{41}{256r_0^2}\int_0^{r_0}\frac{g(r)}{r\{U_\theta^{(0)}(r)\}^2}dr\right],\qquad \text{(D6)}$$

after long but straightforward calculation. The numerical value for the Gaussian vortex ring is $C(\psi_0)/\{\epsilon[U_\theta^{(0)}]^3\}=5.8066\cdots\times10^{-2}>0$. The positivity of $C(\psi_0)$ strongly suggests that a normal mode corresponding to the maximal growth rate exists for the Gaussian vortex ring.

[1] S. E. Widnall and C.-Y. Tsai, "The instability of the thin vortex ring of constant vorticity," Philos. Trans. R. Soc. London, Ser. A **287**, 273 (1977).
[2] S. E. Widnall, D. B. Bliss, and C.-Y. Tsai, "The instability of short waves on a vortex ring," J. Fluid Mech. **66**, 35 (1974).
[3] C.-Y. Tsai and S. E. Widnall, "The stability of short waves on a straight vortex filament in a weak externally imposed strain field," J. Fluid Mech. **73**, 721 (1976).
[4] D. W. Moore and P. G. Saffman, "The instability of a straight vortex filament in a strain field," Proc. R. Soc. London, Ser. A **346**, 413 (1975).
[5] F. Waleffe, "On the three-dimensional instability of strained vortices," Phys. Fluids A **2**, 76 (1990).
[6] Y. Fukumoto and Y. Hattori, "Linear stability of a vortex ring revisited," *Proceedings of the IUTAM Symposium on Tubes, Sheets and Singularities in Fluid Dynamics*, edited by H. K. Moffatt and K. Bajer (Kluwer, New York, 2003), pp. 37–48.
[7] A. Lifschitz and E. Hameiri, "Local stability conditions in fluid dynamics," Phys. Fluids A **3**, 2644 (1991).
[8] S. Friedlander and M. M. Vishik, "Instability criteria for the flow of an inviscid incompressible fluid," Phys. Rev. Lett. **66**, 2204 (1991).
[9] S. Le Dizès and C. Eloy, "Short-wavelength instability of a vortex in a multipolar strain field," Phys. Fluids **11**, 500 (1999).
[10] D. Sipp, E. Lauga, and L. Jacquin, "Vortices in rotating systems: Centrifugal, elliptic and hyperbolic type instabilities," Phys. Fluids **11**, 3716 (1999).
[11] A. Lifschitz, "Instabilities of ideal fluids and related topics," Z. Angew. Math. Mech. **75**, 411 (1995).
[12] A. Lifschitz, W. H. Suters, and J. T. Beale, "The onset of instability in exact vortex rings with swirl," J. Comput. Phys. **129**, 8 (1996).
[13] T. Rozi and Y. Fukumoto, "The most unstable perturbation of wave-packet form inside Hill's vortex," J. Phys. Soc. Jpn. **69**, 2700 (2000).
[14] B. J. Bayly, D. D. Holm, and A. Lifschitz, "Three-dimensional stability of elliptical vortex columns in external strain flows," Philos. Trans. R. Soc. London, Ser. A **354**, 895 (1996).
[15] S. Leblanc, "Destabilization of a vortex by acoustic waves," J. Fluid Mech. **414**, 315 (2000).
[16] E. L. Ince, *Ordinary Differential Equations* (Dover, New York, 1956), Chap. 15.
[17] H. Greenspan, *The Theory of Rotating Fluids* (Cambridge University Press, Cambridge, 1968).
[18] Y. Fukumoto, "Higher-order asymptotic theory for the velocity field induced by an inviscid vortex ring," Fluid Dyn. Res. **30**, 65 (2002).
[19] Y. Fukumoto and H. K. Moffatt, "Motion and expansion of a viscous vortex ring. Part 1. A higher-order asymptotic formula for the velocity," J. Fluid Mech. **417**, 1 (2000).
[20] A. Lifschitz and E. Hameiri, "Localized instabilities of vortex rings with swirl," Commun. Pure Appl. Math. **46**, 1379 (1993).
[21] J. P. Sullivan, S. E. Widnall, and S. Ezekiel, "A study of vortex rings using a laser-Doppler velocimeter," AIAA J. **11**, 1384 (1973).
[22] B. J. Bayly, "Three-dimensional centrifugal-type instabilities in inviscid two-dimensional flows," Phys. Fluids **31**, 56 (1988).